Assessing the Impact of Enhanced Hydrological Processes on Urban Hydrometeorology with Application to Two Cities in Contrasting Climates

JIACHUAN YANG AND ZHI-HUA WANG

School of Sustainable Engineering and the Built Environment, Arizona State University, Tempe, Arizona

MATEI GEORGESCU

School of Geographical Sciences and Urban Planning, Arizona State University, Tempe, Arizona

FEI CHEN AND MUKUL TEWARI

National Center for Atmospheric Research, Boulder, Colorado

(Manuscript received 30 June 2015, in final form 2 January 2016)

ABSTRACT

To enhance the capability of models in better characterizing the urban water cycle, physical parameterizations of urban hydrological processes have been implemented into the single-layer urban canopy model in the widely used Weather Research and Forecasting (WRF) Model. While the new model has been evaluated offline against field measurements at various cities, its performance in online settings via coupling to atmospheric dynamics requires further examination. In this study, the impact of urban hydrological processes on regional hydrometeorology of the fully integrated WRF–urban modeling system for two major cities in the United States, namely, Phoenix and Houston, is assessed. Results show that including hydrological processes improves prediction of the 2-m dewpoint temperature, an indicative measure of coupled thermal and hydrological processes. The implementation of green roof systems as an urban mitigation strategy is then tested at the annual scale. The reduction of environmental temperature and increase of humidity by green roofs indicate strong diurnal and seasonal variations and are significantly affected by geographical and climatic conditions. Comparison with offline studies reveals that land–atmosphere interactions play a crucial role in determining the effect of green roofs.

1. Introduction

To meet the demand of a rapidly growing global population, urban areas have expanded considerably in recent decades (Seto et al. 2011). Through the modification of land surface energy and moisture balances, urbanization has determinant impacts on local and regional hydroclimates, leading to elevated temperature (Arnfield 2003; Yang et al. 2015a), reduced humidity (Unkašević et al. 2001), and change in precipitation patterns (Georgescu et al. 2012). To capture urban land–atmosphere interactions, numerous mesoscale atmosphere–urban modeling systems have been developed in the last decade (Best 2005; Chen et al. 2011; Martilli et al. 2002), among which the Weather Research and Forecasting (WRF) Model–urban system has been widely utilized and examined for major metropolitan regions around the world (Kusaka et al. 2012; Lin et al. 2008; Miao and Chen 2008).

The WRF Model includes several urban parameterization options, including the single-layer urban canopy model (SLUCM), which has been extensively studied and renders satisfactory capability in resolving urban land surface processes with a moderate requirement of input parameter space (Kusaka et al. 2001; Salamanca et al. 2011; Wang et al. 2011a,b). However, because of the oversimplified representation of urban hydrological processes, existing coupled atmosphere–urban modeling systems, including the WRF–SLUCM, have the least capacity in modeling the latent heat flux compared to other fluxes (Grimmond et al. 2010, 2011; Wang et al. 2013). The inadequate urban hydrological modeling

Corresponding author address: Zhi-Hua Wang, School of Sustainable Engineering and the Built Environment, Arizona State University, 501 E. Tyler Mall, P.O. Box 875306, Tempe, AZ 85287-5306.
E-mail: zhwang@asu.edu

DOI: 10.1175/JHM-D-15-0112.1

consequently introduces errors into the atmospheric system via the lower boundary condition, impairing the reliability and accuracy of modeling land–atmosphere interactions (Song and Wang 2015a).

The importance of realistic representation of hydrological processes in the urban canopy model has long been recognized. Aiming at improving prediction of turbulent heat fluxes, Miao and Chen (2014) incorporated urban irrigation, oasis effect, and anthropogenic latent heat into the SLUCM. Evaluation against meteorological observations in Beijing showed that modeled latent heat flux was evidently improved. Inspired by this work and a state-of-the-art urban canopy model (Wang et al. 2011b, 2013), Yang et al. (2015a) further implemented physically based parameterization of evaporation over impervious surfaces and incorporated a green roof system into the SLUCM. Significant enhancement in prediction of latent heat flux was found for the four metropolitan areas investigated: Beijing (China), Vancouver (Canada), Phoenix (United States), and Montreal (Canada). However, tested in an offline (i.e., not dynamically coupled to the overlying atmosphere) setting, this study did not consider the interaction between the land and atmospheric system, and the potential omission of important feedback mechanisms can lead to significant uncertainty and potential errors in model results (Brubaker and Entekhabi 1996).

Using the online WRF–urban modeling system, Georgescu et al. (2011) studied the diurnal cycle of near-surface temperature over the urbanizing Phoenix metropolitan area, concluding that urban irrigation did not have a significant impact on near-surface temperatures. Vahmani and Hogue (2014) assessed the impact of irrigation over the Los Angeles metropolitan area by incorporating an irrigation module into the SLUCM. With irrigation, large biases in prediction of evapotranspiration from urban terrain were reduced. Nevertheless, other urban hydrological processes were neglected in their study, such as anthropogenic latent heat and evaporation from water-holding engineered pavements. It is also noteworthy that the aforementioned studies focused on turbulent heat fluxes, whereas the impact of urban hydrological processes on meteorological variables was rarely quantified. Though turbulent heat fluxes are closely related to temperature and humidity of the atmosphere, the interactions among them are complex with a variety of surface and meteorological conditions (Wang 2014a). Online studies that directly address the effect of hydrological processes on urban meteorology by coupling with the energy balance are still lacking in the literature.

One important function of the mesoscale atmosphere–urban modeling system is to evaluate potential strategies for sustainable cities. Urban areas, owing to impacts of global climate change, are projected to experience more frequent occurrences of climatic extremes in the future [e.g., heat wave (Meehl and Tebaldi 2004) and strong precipitation (Kripalani et al. 2007)], increasing the need for sustainable adaptation/mitigation strategies in areas where the majority of the globe's inhabitants reside (IPCC 2012; Georgescu et al. 2014). Green (vegetated) roofs have significant potential and have been adopted in many cities (e.g., Chicago) to alleviate urban-induced heat stresses. The adoption of green roofs has been shown to reduce near-surface temperature (Yang and Wang 2014, 2015; Georgescu 2015), improve stormwater management (VanWoert et al. 2005; Carter and Jackson 2007), and enhance air quality (Yang et al. 2008; Rowe 2011). Although researches on meteorological impacts of green roofs are becoming increasingly widespread, most investigations have focused on building-resolving scales and explored with offline models where meteorological forcing is provided as boundary conditions (Sailor 2008; Sun et al. 2013). Upscaling the results of these studies for preparing guidance on green roof implementation for a city or at regional scales remains challenging because of the substantial influence of surface heterogeneity and land–atmosphere interactions (Ramamurthy et al. 2014; Song and Wang 2015b).

Consequently, there have been only a handful of studies investigating climatic (Georgescu et al. 2014; Georgescu 2015) and meteorological (Li et al. 2014) impacts of green roofs in a coupled atmosphere–urban modeling framework. Georgescu et al. (2014) explored the benefits of green roofs relative to highly reflective roofs and the potential to offset urban-induced warming at seasonal and annual time scales across the contiguous United States. Although impacts on near-surface temperature were less for green roofs relative to reflective roofs, a considerably reduced hydroclimatological tradeoff was simulated for several regions via deployment of vegetated roofs. However, assuming green roofs were infinitely evaporating without water constraint, their results represented the maximum potential benefits of evaporating rooftop water pools rather than green roofs. Li et al. (2014) also compared the effectiveness of green roofs with white roofs by coupling the Princeton urban canopy model into the WRF system. They focused on a 3-day summer heat wave event, whereas the long-term performance of green roofs was not addressed. More importantly, urban hydrological processes were not adequately represented in these studies (urban irrigation,

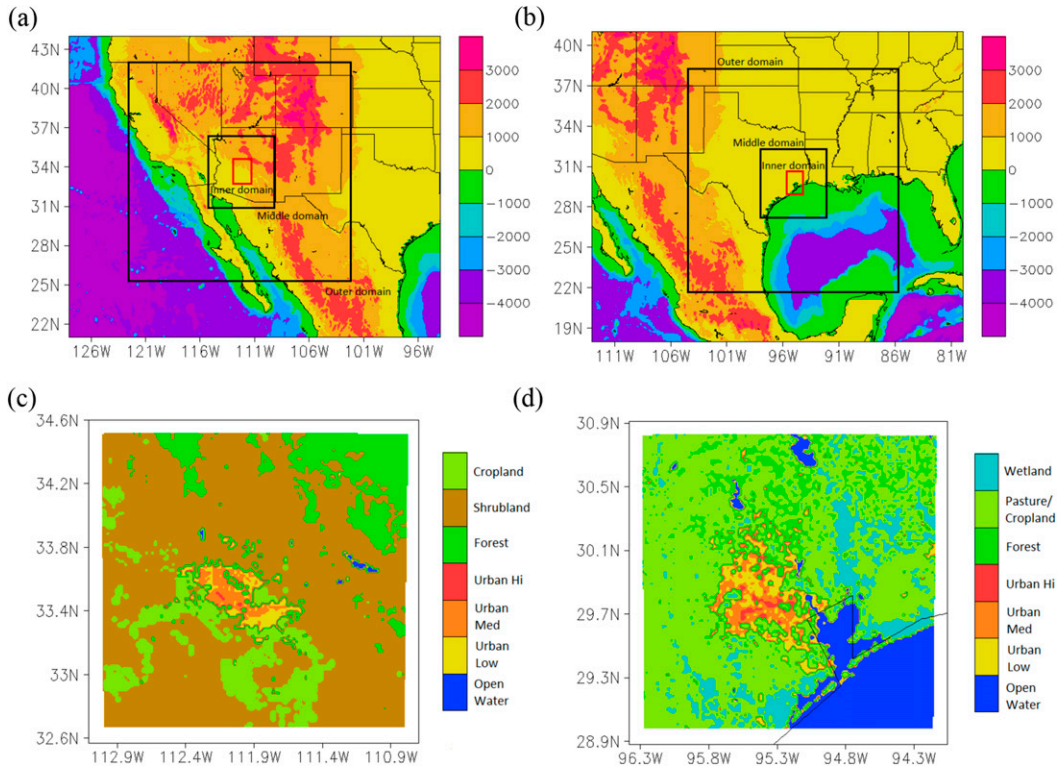

FIG. 1. Geographical representation of the domain extent with topography (m) overlaid for (a) Phoenix and (b) Houston. Land-use/land-cover information of the inner domain for (c) Phoenix and (d) Houston.

oasis effect, etc.), leading to potential uncertainties in the findings.

It is therefore imperative to implement urban hydrological processes into a coupled atmosphere–urban modeling system to investigate their impacts under a fully interacting environment. Enabled by the realistic resolution of urban hydrological processes in a recent study (Yang et al. 2015a), here we use the enhanced integrated WRF–urban modeling system to 1) evaluate the impact of hydrological processes on prediction of urban hydrometeorological variables and 2) assess the effect of green roofs at the regional scale with seasonal variability. To investigate model results under different geographical and climatic conditions, simulations are conducted for two major cities in the United States, namely, Phoenix and Houston.

2. Methodology

a. WRF–urban modeling system

WRF is a fully compressible, nonhydrostatic modeling system that has been used for a variety of applications, ranging from local to global scale (Skamarock and Klemp 2008). Here we used WRF, version 3.4.1, to conduct simulations over study metropolitan areas. Initial meteorological conditions for the WRF simulations were obtained from the National Centers for Environmental Prediction Final Operational Global Analysis data, which were available on a 1° × 1° resolution with a 6-h temporal frequency (details can be found on http://rda.ucar.edu/datasets/ds083.2/). The Noah land surface model, coupled with the single-layer urban canopy model, was used to simulate land surface processes after initiation. Note that we adopted an enhanced version of SLUCM, which

TABLE 1. Summary of numerical experiments performed.

Case No.	Model	Hydrological process
1	Old SLUCM	Same as default WRF, version 3.4.1
2	New SLUCM	Case 1 + anthropogenic latent heat + urban irrigation + evaporation from water-holding engineered pavements + urban oasis effect
3	New SLUCM	Case 2 + multilayer green roof system

TABLE 2. Summary of name, location, and land-use type of meteorological stations used in this study.

Station name	Source	Lat (°N)	Lon (°W)	Land use
Phoenix				
Encanto	AZMET	33.479	112.096	Urban
Mesa	AZMET	33.387	111.867	Urban
Sky Harbor Airport	NCEI	33.428	112.004	Urban
Buckeye	AZMET	33.400	112.683	Rural
Waddell	AZMET	33.618	112.460	Rural
Greenway	AZMET	33.621	112.108	Rural
Desert ridge	AZMET	33.733	111.967	Rural
Houston				
Pearland	NCEI	29.519	95.242	Urban
D.W. Hooks	NCEI	30.068	95.556	Urban
William	NCEI	29.638	95.282	Urban
Intercontin	NCEI	29.980	95.360	Rural
Suger	NCEI	29.622	95.657	Rural

featured the integration of 1) anthropogenic latent heat, 2) urban irrigation, 3) evaporation from water-holding engineered pavements, 4) urban oasis effect, and 5) multilayer green roof system. Detailed information of individual processes can be found in previous work (Yang et al. 2015a). Other major physical parameterization schemes used in this study include: 1) the new Thompson scheme for microphysics (Thompson et al. 2008), 2) the Rapid Radiative Transfer Model for longwave radiation (Mlawer et al. 1997), 3) the Dudhia scheme for shortwave radiation (Dudhia 1989), 4) the MM5 similarity scheme for surface layer, and 5) the Yonsei University scheme for planetary boundary layer (Hong et al. 2006). Cumulus parameterization is turned on only for the outer and middle domain, using the Kain–Fritsch scheme (Kain 2004).

b. Experiment design

To compare the effect of urban hydrological processes under different geographical and climatic conditions, we selected Phoenix and Houston as our study sites. These two are among the top 10 most populous cities in the United States, whose urban heat island and hydroclimate has been extensively studied in the literature (Georgescu et al. 2012; Salamanca et al. 2011; Yang et al. 2015b).

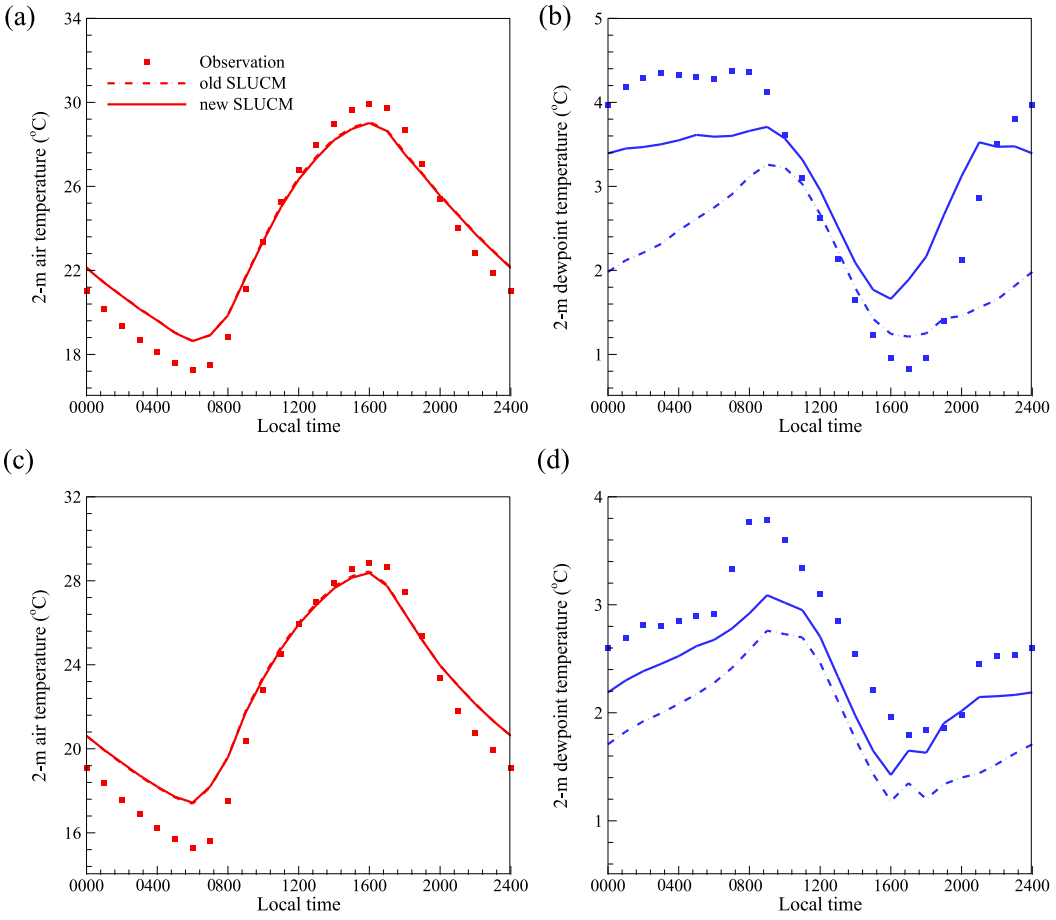

FIG. 2. Comparison of annual average diurnal profiles of simulated and observed (a) urban T_2, (b) urban T_{d_2}, (c) rural T_2, and (d) rural T_{d_2} for Phoenix.

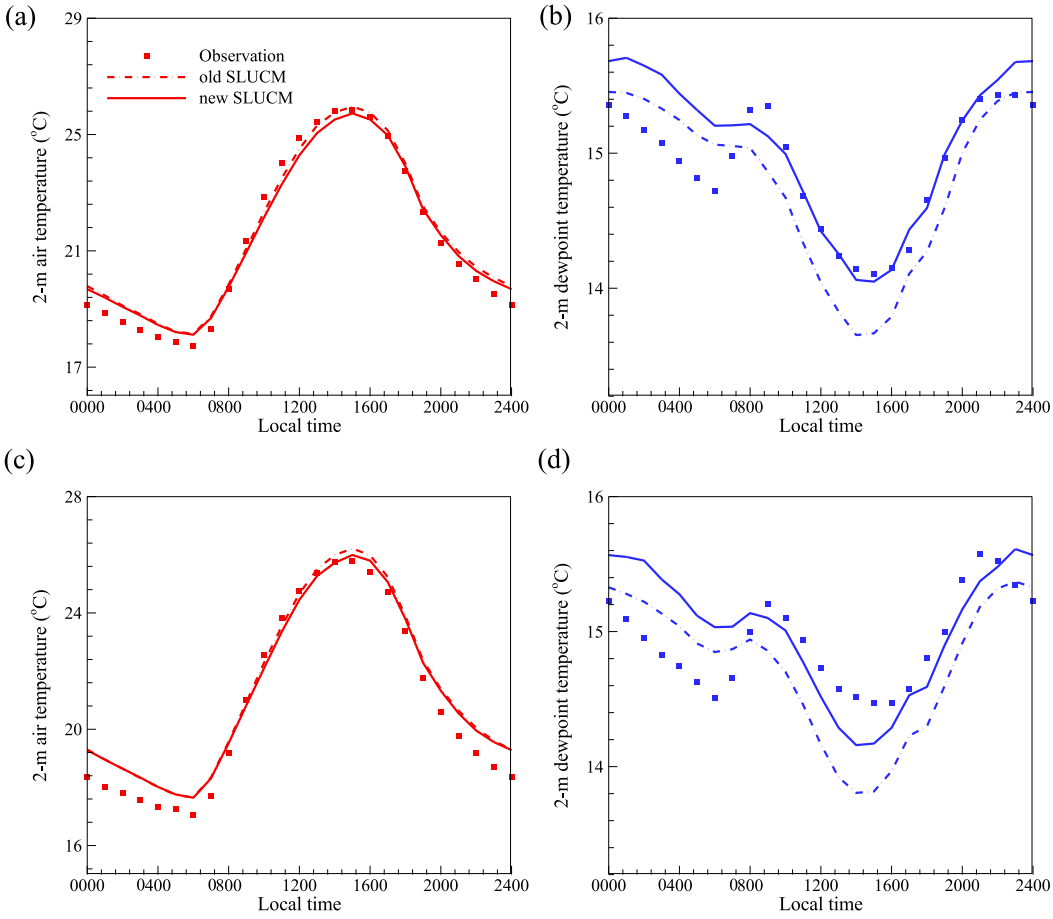

FIG. 3. Comparison of annual average diurnal profiles of simulated and observed (a) urban T_2, (b) urban T_{d_2}, (c) rural T_2, and (d) rural T_{d_2} for Houston.

Distinct conditions in two regions (e.g., inland semiarid for Phoenix and coastal humid for Houston) facilitate a better understanding of urban hydrological processes under different geographical and climatic conditions.

For both areas, we used a two-way nested grid configuration with all three domains centered on the city (see Figs. 1a,b). Spatial resolution for the outer, middle, and inner domains was 32, 8, and 2 km, respectively. The outer domain covered a surface area of 1856 km × 1856 km, and the inner domain had a size of 212 km × 212 km. As the outer and middle domains cover portions of Mexico, MODIS global land-cover data were used (Friedl et al. 2002). For the inner domain, we used the National Land Cover Database (NLCD) 2006 (Fry et al. 2011) to represent the heterogeneous urban landscape that is subdivided into three categories (see Figs. 1c,d). We selected year 2006 for this study to represent a normal annual climatic condition for both cities. Simulations were initiated at 0000 UTC 1 November 2005 and concluded at 0000 UTC 1 December 2006. November 2005 was the spinup period and was not included in the subsequent analysis. Considering the time span of simulations and geographical locations, sea surface temperature was updated at an interval of 1 day. In this study, our analysis focused on the inner domain, and results of the other two domains are not discussed.

For each city, a total of three sets of simulation were conducted (see Table 1). The first case was a control run with the default SLUCM (hereafter "old SLUCM") in WRF. The second case employed the recently enhanced SLUCM (Yang et al. 2015a; hereafter "new SLUCM") with a more realistic representation of urban hydrological processes. The last case assumed a 100% areal fraction of green roof deployment over the study cities using the new SLUCM. With this experiment design, the impact of hydrological processes can be readily obtained by comparing results from the first and second cases. The difference in results between the second and last cases renders the regional impact of green roofs.

TABLE 3. Summary of average daily max, mean, and min T_{d_2} (°C) for different seasons. Obs is short for observation; Old and New denote simulation results with the old and new SLUCM, respectively.

	Daily max			Daily mean			Daily min		
	Obs	Old	New	Obs	Old	New	Obs	Old	New
Phoenix									
DJF	−1.91	−3.15	−1.61	−5.71	−6.63	−5.50	−9.12	−10.22	−9.28
MAM	4.69	3.67	4.10	0.62	−0.07	0.36	−3.66	−3.75	−3.37
JJA	15.54	13.02	13.33	11.81	10.36	10.64	7.83	7.68	7.93
SON	8.86	7.87	8.49	4.92	4.52	5.18	0.94	1.15	1.79
Houston									
DJF	10.94	11.51	11.92	6.25	6.27	6.8	1.58	1.15	1.74
MAM	18.25	19.65	19.75	15.64	15.9	16.02	12.47	11.79	11.93
JJA	23.54	22.41	22.45	22.01	19.76	19.83	20.1	15.84	15.94
SON	18.57	18.22	18.47	15.59	14.17	14.44	12.25	9.89	10.27

3. Impact of urban hydrological processes

Performance of the WRF simulations was evaluated against hourly meteorological observations from ground-based weather stations. Simulated 2-m air temperature T_2 and 2-m dewpoint temperature T_{d_2} at 1-h frequency were available for direct comparison to observed data. These two variables were selected because of their importance in fire weather prediction (Cheng and Steenburgh 2005). Besides, they are essential inputs to a variety of hydrological and ecological models for resolving evapotranspiration processes and plant productivity (Dodson and Marks 1997). For Phoenix, we utilized data from the Arizona Meteorological Network (AZMET) and NOAA's National Centers for Environmental Information (NCEI). Details of the meteorological stations are summarized in Table 2. Based on NLCD 2006 land-use classification, four stations were identified as urban and the rest as rural. In Houston, only data from NCEI were used, among which three stations were urban and two were

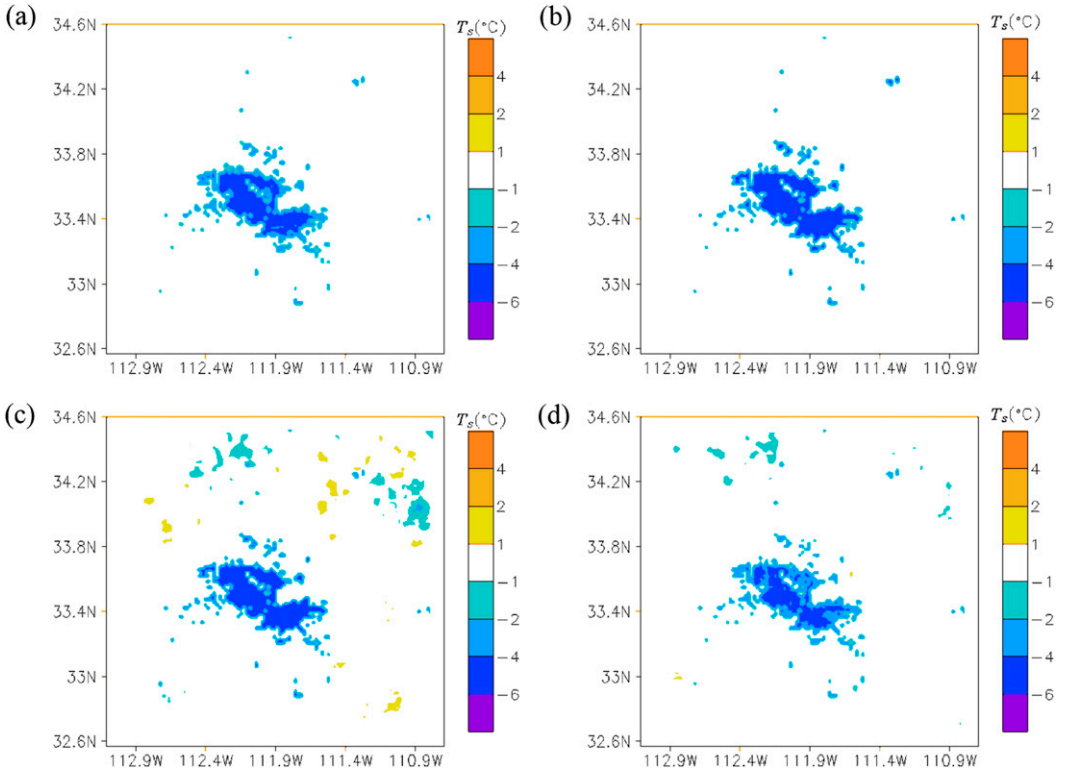

FIG. 4. Simulated impact of green roofs on land surface temperature at 1400 LT for Phoenix during (a) winter, (b) spring, (c) summer, and (d) fall.

TABLE 4. Summary of observed (Obs is short for observation) and simulated precipitation (mm) for different seasons at the two study areas.

	Obs	New SLUCM with green roofs	No green roof
Phoenix			
DJF	1.6	4.8	4.8
MAM	39.7	47.9	46.5
JJA	82.3	59.4	55.6
SON	79.4	100.5	99.0
Houston			
DJF	185.7	134.5	132.8
MAM	141.2	172.7	165.3
JJA	307.6	205.3	202.7
SON	365.5	301.6	268.7

rural. Arithmetic average of ground-based measurements is compared against that of simulation results at corresponding model grids for evaluation.

Figure 2 compares the simulated annual average diurnal profiles of T_2 and T_{d_2} with the old and new SLUCM against the observations for Phoenix. Hydrological processes are expected to reduce air temperature and increase dewpoint temperature at the 2-m level of urban areas; nevertheless, Fig. 2 shows that the effect on 2-m air temperature is negligible. One important reason for this phenomenon is the limited effective area and time of hydrological processes. Among the implemented urban hydrological processes, urban irrigation and oasis effect are effective over vegetated area, which is only 20% of the urban land surface in Phoenix. Evaporation from water-holding engineered pavements functions during and shortly after rainfall; therefore, its long-term average impact is trivial. Another critical reason is the parameterization schemes used in the WRF Model. The WRF Model adopts a "tile" approach, where fluxes over built and vegetated surfaces are weighted by their respective areal fractions to calculate the total flux arise from the urban land surface. In this case, surface and air temperatures are largely determined by the built surface, whose areal fraction and temperature are significantly larger than those over the vegetated surface. Anthropogenic latent heat is directly added to the latent heat flux term so that it does not directly participate into the urban surface energy balance via the distribution of available solar radiation to dispersive and ground heat. On the other hand, moisture and humidity over the urban land surface are primarily controlled by vegetation, as there is no evaporation over the built surface most of the time.

In terms of T_{d_2}, it is clear from Fig. 2 that modeled T_{d_2} is significantly underestimated in WRF simulations with

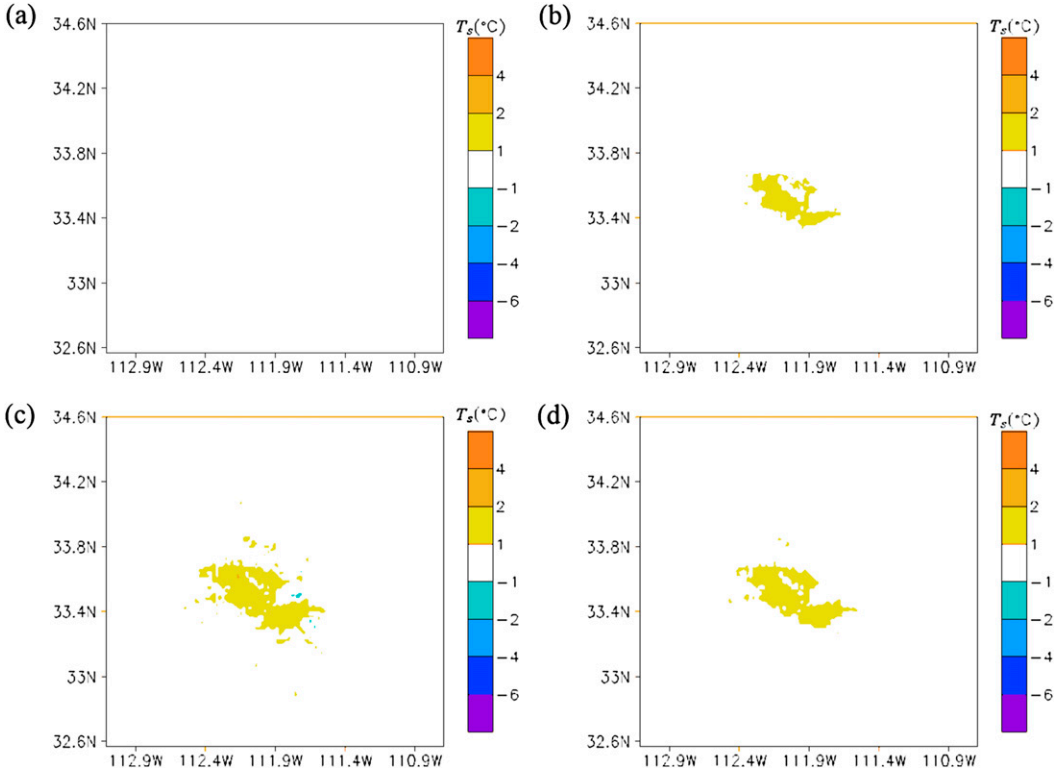

FIG. 5. Simulated impact of green roofs on land surface temperature at 0200 LT for Phoenix during (a) winter, (b) spring, (c) summer, and (d) fall.

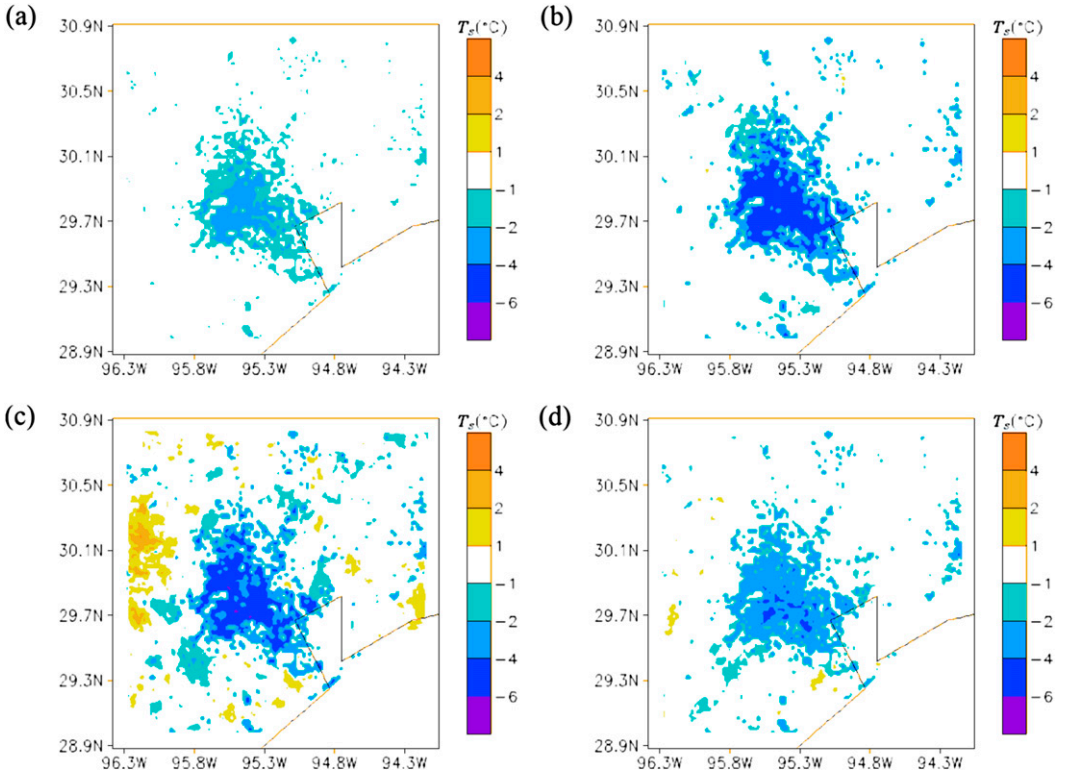

FIG. 6. Simulated impact of green roofs on land surface temperature at 1400 LT for Houston during (a) winter, (b) spring, (c) summer, and (d) fall.

the old SLUCM. Diurnal minimum T_{d_2} is found at 1600 local time (LT), which corresponds to maximum T_2. Incorporating urban hydrological processes, model prediction agrees better with observations. Increase of T_{d_2} can be up to about 1.5°C for the urban area across the diurnal cycle. Via urban–rural circulations, urban hydrological processes also have detectable effects on rural T_{d_2}, though with a smaller magnitude. Results for Houston are plotted in Fig. 3. Located in a coastal area, Houston has a lower air temperature and a higher dewpoint temperature than Phoenix. Daytime onshore flow provides moisture for the urban area and therefore weakens the influence of urban hydrological processes. Increase in T_{d_2} by hydrological processes is about 0.3°C for Houston.

Figures 2 and 3 illustrate that urban hydrological processes have limited effects on T_2. Hence, we used the daily maximum, mean, and minimum 2-m dewpoint temperatures for statistical analysis. Evaluating these temperatures is very useful as they are indices for climate extremes (Alexander et al. 2006; Perkins et al. 2007). Seasonally averaged results for Phoenix and Houston are summarized in Table 3, which shows that with the old SLUCM, WRF simulations considerably underestimate daily maximum and mean T_{d_2}. The new SLUCM with enhanced urban hydrological modeling enables improved predictions for the entire simulation period.

For Phoenix, increase in daily maximum and mean T_{d_2} is about 1.2°, 0.4°, 0.3°, and 0.6°C for winter [December–February (DJF)], spring [March–May (MAM)], summer [June–August (JJA)], and fall [September–November (SON)], respectively. With respect to daily minimum T_{d_2}, the improvement is less clear. Improvement is observed in winter while degradation is reported for fall. In Houston, the impact of urban hydrological processes is weak because of the presence of sea–land breezes. During spring and summer when temperature difference is distinct between the land and sea surface, strong onshore flow makes the effect of urban hydrological processes negligible. For fall and winter, average daily maximum, mean, and minimum T_{d_2} is increased by about 0.6° and 0.3°C, respectively.

4. Regional hydroclimatic effect of green roofs

Using the model with enhanced urban hydrology, here we conducted simulations to investigate the regional effect of green roofs for both Phoenix and Houston. Our hypothetical scenario assumes that all rooftops of the two cities are replaced by green roofs, with results indicating

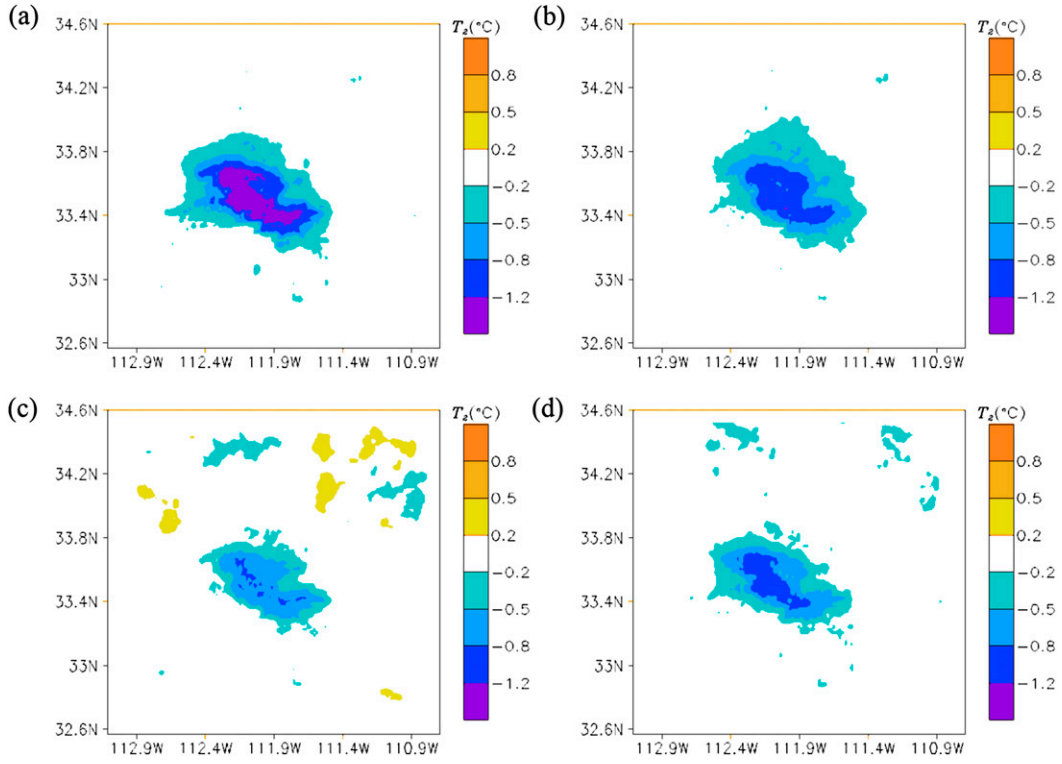

FIG. 7. Simulated impact of green roofs on 2-m air temperature at 1400 LT for Phoenix during (a) winter, (b) spring, (c) summer, and (d) fall.

the maximum possible effect. Here we select short grasses for green roof vegetation type with a 0.3-m deep loam soil layer. Sensitivity of green roof performance to parameters related to soil and vegetation type is referred to the previous study (Yang and Wang 2014).

Figure 4 shows the seasonal variability of impacts of green roofs on land surface temperature T_s at 1400 LT for Phoenix. We present the result at 1400 LT, as subsequent analysis finds the time corresponds to diurnal maximum effect (see Fig. 13, described in greater detail below). From Fig. 4, it is clear that green roofs can reduce T_s of the urban area by more than 4°C throughout the year (cf. Fig. 1c for the urban area in Phoenix). Compared to other seasons, fall (SON) has the smallest reduction in T_s, primarily because of the extensive amount of precipitation simulated in this season. Simulated accumulated precipitation depth for spring, summer, fall, and winter is about 47.9, 59.4, 100.5, and 4.8 mm, respectively. Seasonal variation of precipitation in the case with implemented green roofs is similar to that of the control case (see Table 4). Compared to in situ measurements, model prediction underestimates precipitation in summer and overestimates it in fall for Phoenix. The deviation in precipitation pattern can be caused by various physical parameterizations, such as microphysics, planetary boundary layer, and cumulus schemes. Closing the gap between simulated and observed precipitation requires a thorough sensitivity analysis in the future and is beyond the scope of this study.

In a previous offline study, Yang et al. (2015a) reported a green roof cooling of the Phoenix metropolitan area by about 8°C at 1400 LT in summer. This significant difference between offline and online simulation results indicates that feedback between the atmospheric system and land surface has notable influences on the performance of green roofs. Results in this study, derived from the fully coupled WRF–urban modeling system, are more representative of actual effects. To demonstrate impacts during nighttime hours, results at 0200 LT are shown in Fig. 5. With additional soil layers on top of buildings, green roofs are able to store extra solar energy during daytime as compared to conventional roofs. The energy is released and causes a considerable warming effect at night. Figure 5 demonstrates that increase in T_s is about 1°–2°C from spring to fall and is less than 1°C in winter. The magnitude of nighttime warming is much smaller than that of daytime cooling by green roofs for Phoenix. These results are consistent with recent high-resolution simulations for urbanizing regions in California, which similarly indicated an increased nighttime warming

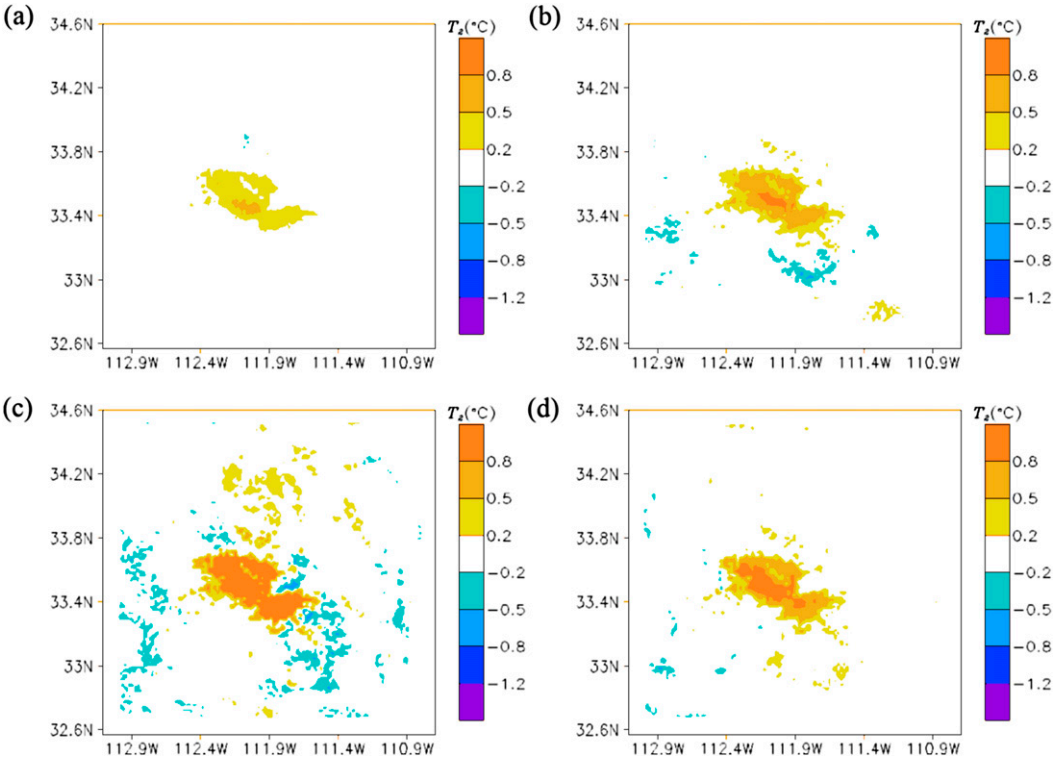

FIG. 8. Simulated impact of green roofs on 2-m air temperature at 0200 LT for Phoenix during (a) winter, (b) spring, (c) summer, and (d) fall.

tendency for green roofs deployment that was considerably smaller in magnitude relative to daytime cooling (Georgescu 2015).

Cooling effect of green roofs on T_s at 1400 LT for Houston is shown in Fig. 6 (cf. Fig. 1d for the urban area in Houston). Compared to Phoenix, temperature reduction in fall and winter for Houston is much lower. Evaporative cooling of green roofs is mainly controlled by two factors: available energy and availability of water at the surface. As precipitation for Houston is abundant throughout the year, evapotranspiration arising from green roofs is largely determined by the available solar radiation. Houston is known to have a much cloudier weather and thus less total available solar radiation than the desert city Phoenix. In winter, when the sun angle is lower, solar radiation intensity decreases significantly and green roofs become relatively less effective. Precipitation also plays a role in determining the cooling effect. During the simulation period, Houston receives nearly double the amount of rainfall in fall as compared to spring (see Table 4), which indicates fewer clear days on average, leading to ineffectiveness of green roofs.

Difference in simulated 2-m air temperature between 0% and 100% green roof fraction cases at 1400 LT for Phoenix is shown in Fig. 7. Opposite to the trend of surface temperature, it is found that the strongest cooling effect on T_2 of more than 1.2°C occurs in winter, while the smallest reduction is less than 0.8°C in summer. A reason for this phenomenon is that nonlinear relation exists between surface temperature and 2-m air temperature. When green roofs reduce T_s, buoyancy effect is also reduced such that the reduction of T_2 is smaller than the reduction of T_s. Another critical factor contributing to the phenomenon is the warming effect caused by green roofs at night, as demonstrated in Fig. 8. Compared to winter, the urban land surface in summer receives a considerably enhanced solar radiative flux, which is stored via a large thermal mass of manmade structures and is subsequently released at night. In the absence of incoming solar radiation, vertical mixing over urban terrain in nighttime is weak so that the evolution of air temperature is steady (Poulos et al. 2002). As a consequence, increase in T_2 by heat released from green roofs dissipates slowly until sunrise when surface heating modifies the stability condition of the boundary layer. Figure 8 clearly illustrates that increase in T_2 in summer is more significant than that in winter, in terms of both the influence area and the magnitude. This nighttime warming impedes cooling of air temperature in daytime and results in the stronger cooling of T_2 in winter as compared to summer.

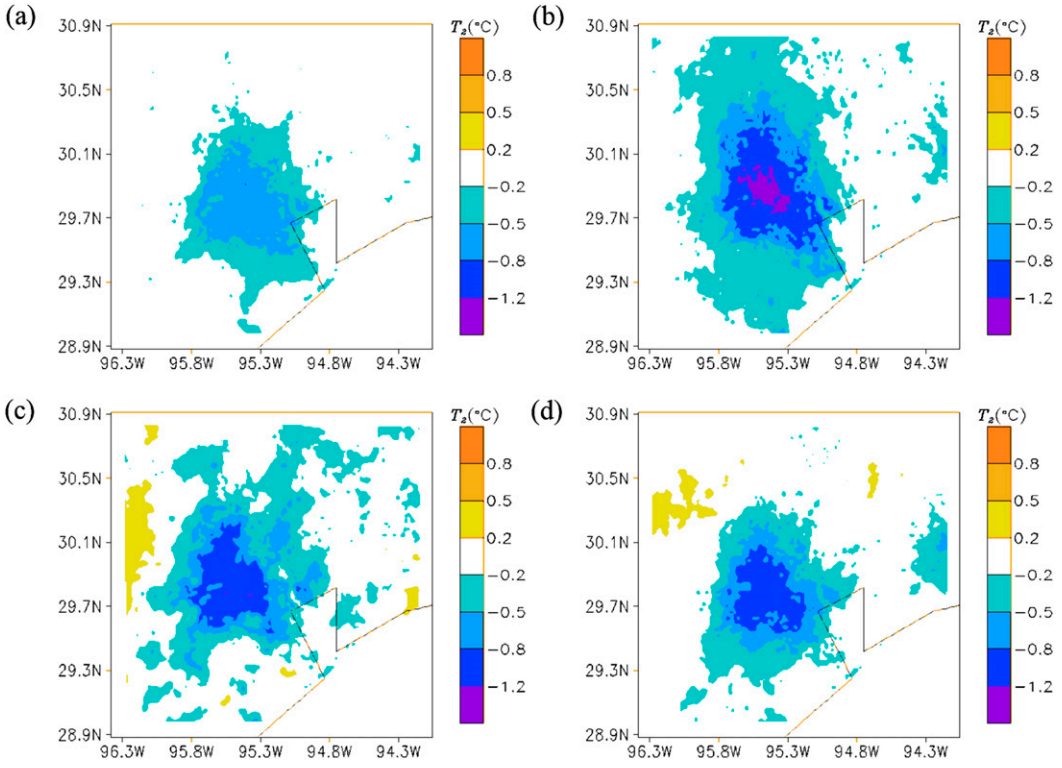

FIG. 9. Simulated impact of green roofs on 2-m air temperature at 1400 LT for Houston during (a) winter, (b) spring, (c) summer, and (d) fall.

Figure 9 demonstrates the regional effect of green roofs on T_2 at 1400 LT for Houston. It is noteworthy that unlike in Phoenix, the order of reduction in T_2 among different seasons generally follows that of T_s for Houston. This is primarily due to the negligible nighttime warming of air temperature in Houston throughout the year (results not shown here). In a coastal area, different surface cooling over land and sea results in a temperature gap in overlying air layers and consequently leads to nighttime advection of marine air. Simulated results of the 10-m wind speed at 2100 LT (sunset around 2000 LT) for Houston during summer are presented in Fig. 10. Advection of marine air toward the land tends to reduce T_2 over sea and increase T_2 over land. As illustrated in Fig. 8, green roofs tend to increase T_2 over urban areas at night. The increase in urban T_2 reduces the land–sea air temperature difference, weakens the nocturnal advection, and eventually offsets the warming effect on T_2 over urban areas. Figure 10 shows that green roofs decrease 10-m wind speed by about 1 m s^{-1} in the bay

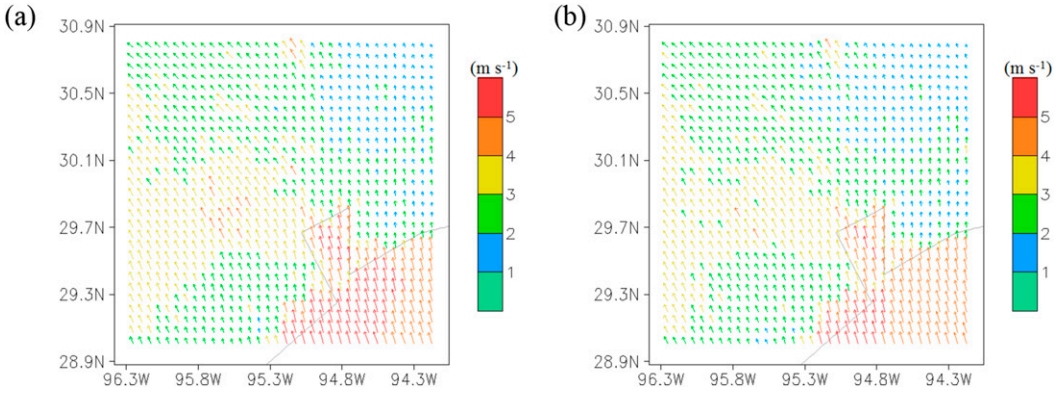

FIG. 10. Simulated 10-m wind speed at 2100 LT for Houston during summer: (a) control case without green roofs and (b) green roof case.

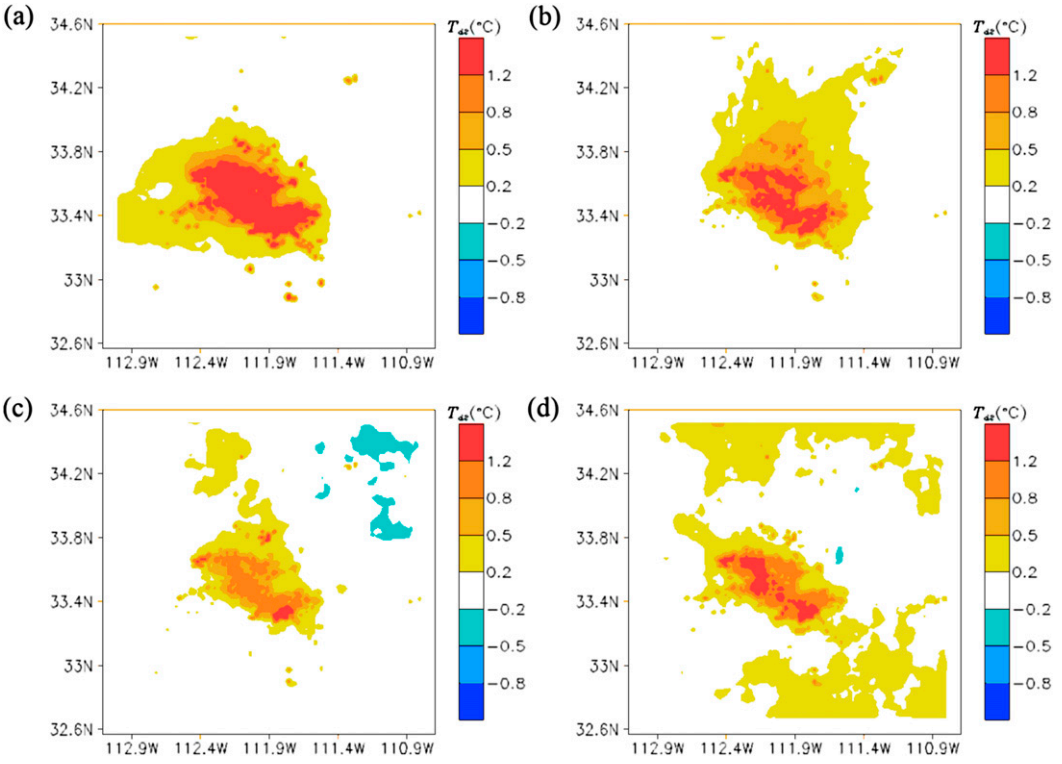

FIG. 11. Simulated impact of green roofs on 2-m dewpoint temperature at 1400 LT for Phoenix during (a) winter, (b) spring, (c) summer, and (d) fall.

area. The combined effect of green roofs on nocturnal T_2 is therefore insignificant. With an insignificant nighttime warming, daytime cooling of T_2 follows the trend of reduction in T_s. Reduction in T_2 at 1400 LT for Houston is less than 0.8°C in winter and can be up to more than 1.2°C in summer. It is worth mentioning that the cooling effect on T_2 has a larger spatial coverage in Houston because of the existence of land–sea circulation, especially in spring and summer when there is a considerable gap between land and sea surface temperature.

Impact of green roofs on 2-m dewpoint temperature for Phoenix at 1400 LT is shown in Fig. 11. Through evaporative cooling, green roofs are able to increase moisture and decrease temperature of the near-surface air layer, thus leading to a substantial rise in T_{d_2} for the entire simulation period. Sunwoo et al. (2006a,b) suggested relative humidity should be maintained at greater than 30% to avoid dryness of the eyes and skin. Therefore, increased air humidity can enhance the thermal comfort of pedestrians in a dry environment, such as the premonsoon season in Phoenix (relative humidity ≈ 12%). However, extra moisture in the monsoon season can aggravate the thermal discomfort of residents, as illustrated in a recent study on urban irrigation (Yang and Wang 2015). This two-sided effect of green roofs needs special attention, especially in humid regions like Houston. Figure 11 demonstrates that increase of T_{d_2} can be up to more than 1.2°C across the year. It is easy to recognize that seasonal variation of the increase in T_{d_2} is similar to that of the decrease in T_2 for Phoenix because of the nonlinear relationship between saturated vapor pressure with air temperature. According to the Clausius–Clapeyron equation, a same amount of increase in absolute humidity of air will cause a larger increase of dewpoint temperature at a lower air temperature. At night, the evapotranspiration rate becomes much slower as the driving force (solar radiation) disappears, and thus the influence of green roofs on T_{d_2} becomes insignificant (results not shown here). Figure 12 presents the results at 1400 LT for Houston. The relation between green roofs' effects on T_{d_2} and T_2 is consistent in both cities.

Besides spatial variation, temporal variation of the impact of green roofs is investigated. Realizing the maximum and minimum effects of green roofs in a temporal cycle has important implications for urban planning. In fact, the time at which spatial effect of green roofs was presented (e.g., 1400 and 0200 LT in above context) is selected based on diurnal results in Fig. 13. Figure 13 demonstrates the diurnal impact of green roofs averaged over the entire Phoenix urban area. As expected, latent heat flux (LE) from green roofs increases with intensity of solar radiation at the surface, and the largest increment

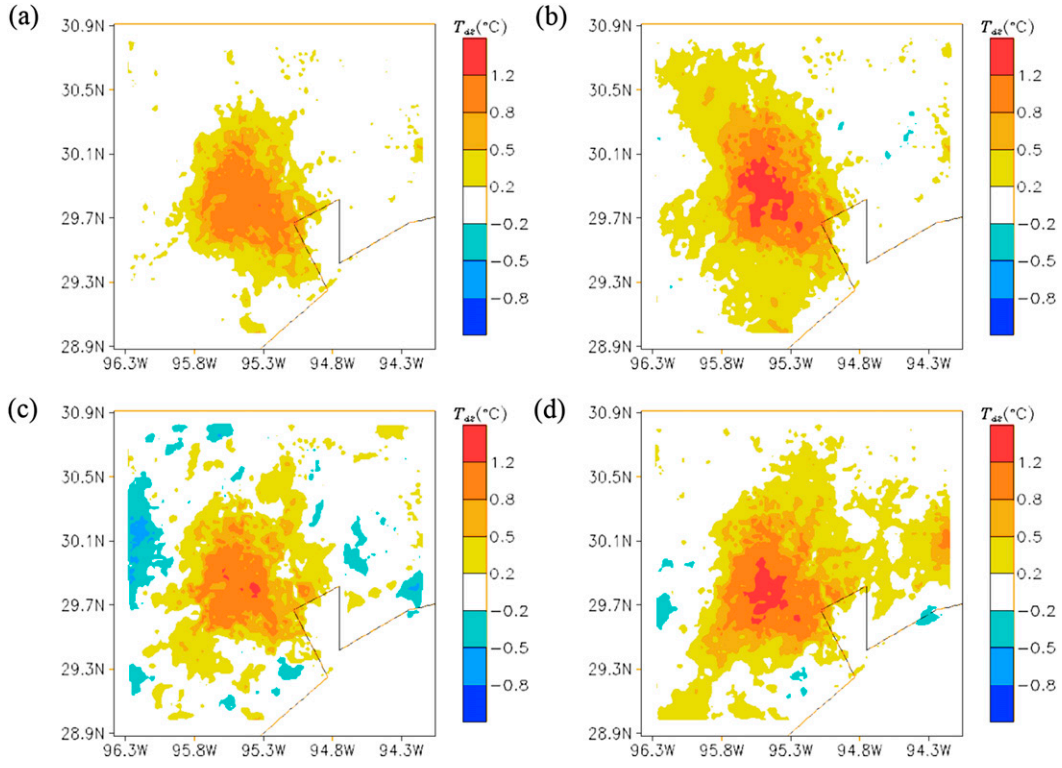

FIG. 12. Simulated impact of green roofs on 2-m dewpoint temperature at 1400 LT for Houston during (a) winter, (b) spring, (c) summer, and (d) fall.

of more than 70 W m^{-2} is found in summer. Additionally, daytime sunshine duration controls the effective period of green roofs. It is indicated from Fig. 13a that green roofs function about 4 h more in summer than in winter.

While the increase in LE is the largest in summer, it does not necessarily lead to the greatest reduction in T_s. As shown in Fig. 13b, the strongest cooling of the urban land surface by green roofs occurs in spring instead of summer, owing to the monsoon period from July to September in Arizona. The extensive amount of precipitation in fall also results in a smaller reduction of T_s than that in winter. With respect to the nighttime warming, the increase of T_s by green roofs from the largest to the smallest is in summer, fall, spring, and winter. The order is the same for the increase in nighttime T_2. The average increment of nighttime T_2 is about 1.1°C in summer and about 0.3°C in winter. As mentioned, the difference in nighttime warming has significant implications for the daytime cooling process. Consequently, the largest reduction of daytime T_2 and the largest increase of T_{d_2} by green roofs occur in winter. In this particular period from December 2015 to February 2016, Phoenix was abnormally dry, leading to low evapotranspiration from green roofs, such that a few rainfall events in this period cause the spike in latent heat flux in Fig. 13d.

The average impact of green roofs on studied variables for Houston is qualitatively similar to that for Phoenix; however, the seasonal variation of the impact differs considerably. With sufficient supply of water from precipitation, effectiveness of green roofs in Houston largely depends on the duration and strength of incoming solar radiation. Figure 14a shows that increased LE by green roofs can be up to more than 130 W m^{-2} in spring and summer, which is remarkably larger than the increase of about 80 W m^{-2} in fall. With respect to T_s, Fig. 14b demonstrates that daytime cooling effect is the strongest in summer and the weakest in winter, while nighttime warming is almost negligible. Diurnal impact of green roofs on T_2 across various seasons is similar to that on T_s. The peak cooling effect is found to be about 1°C in spring and summer. As land–sea circulation mixes the air layer of coastal area, increased T_{d_2} by green roofs has a relatively limited seasonal variation.

5. Concluding remarks

In this study, we applied the WRF Model framework with an enhanced single-layer urban canopy model to assess the effect of hydrological processes on urban hydrometeorology. Evaluation against field measurements

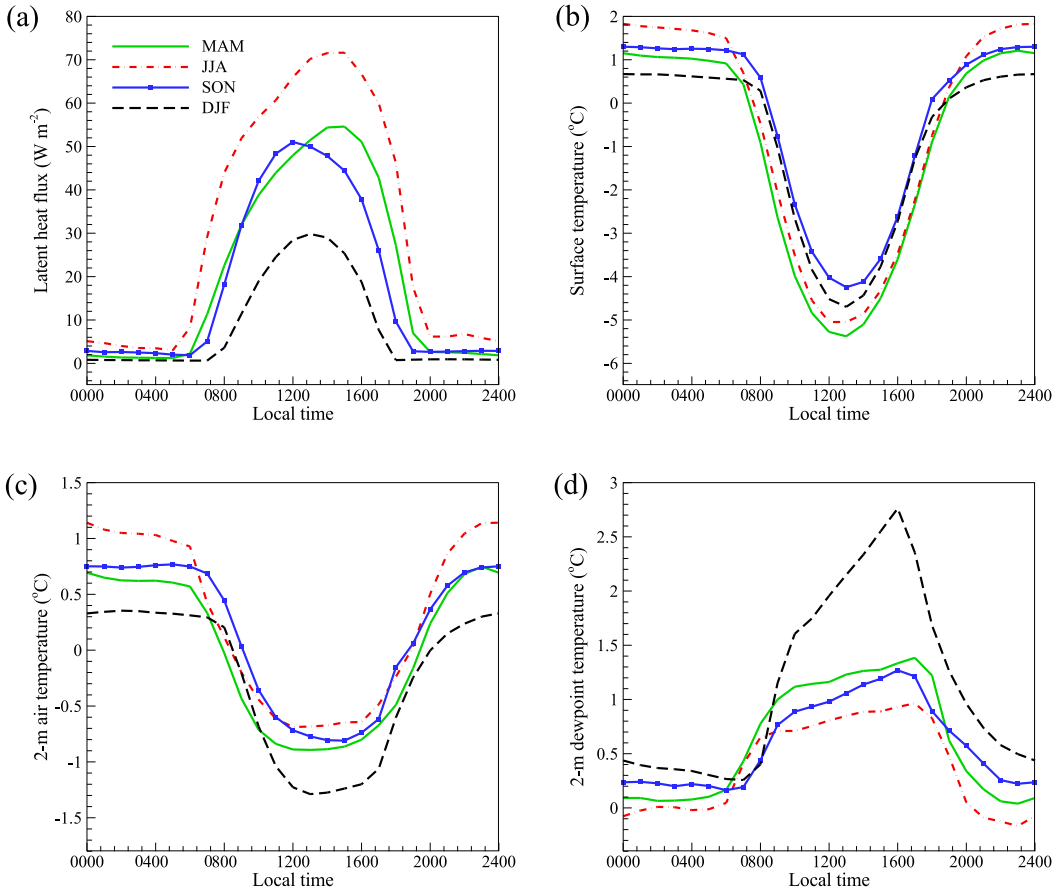

FIG. 13. Diurnal variation of average impact of green roofs on (a) LE, (b) T_s, (c) T_2, and (d) T_{d_2} over the entire Phoenix metropolitan area.

illustrates that more realistic representation of urban hydrological processes improves the prediction of the 2-m dewpoint temperature. Results of regional hydroclimate simulations indicate that green roofs are effective in reducing daytime air temperature and increasing dewpoint temperature over urban areas. The impact of green roofs exhibits strong diurnal and seasonal variability and depends on geographical and climatic conditions. It is noteworthy that urban vegetation is largely represented as grasses and short corps in the WRF–urban modeling system, whereas physical resolution of more diverse urban vegetation types, for example, tall trees, and their hydrometeorological effect, such as on radiative energy exchange, remains an open challenge in regional simulations (Krayenhoff et al. 2014; Wang 2014b; Wang et al. 2016).

Numerical experiments clearly demonstrate the effect of urban hydrological processes for Phoenix and Houston in this study. However, with a limited computational resource, uncertainty of simulation results is not adequately addressed after fulfilling the fine spatial resolution and long simulation period in experimental setup. The uncertainty consists mainly of two parts: 1) sensitivity of model results to initial and boundary conditions and 2) sensitivity to physical parameterizations in the WRF Model. To reduce the uncertainty and provide a better quantitative estimation of the effect, an ensemble approach will be needed in future work.

Comparing results from this study and a previous offline study, it is indicated that land–atmosphere interactions cannot be ignored in quantifying the influence of surface hydrological process. In the coastal area, land–sea circulation mixes the near-surface air layer, leading to a weaker effect of hydrological processes on the meteorological field than that of the inland area. To accurately evaluate sustainable adaptation/mitigation strategies for urban areas, numerical experiments should be carried out with a fully interacting land–atmosphere modeling system. In addition, modification of urban landscape will have strong implications for hydrometeorology of surrounding rural areas, necessitating serious consideration and planning prior to

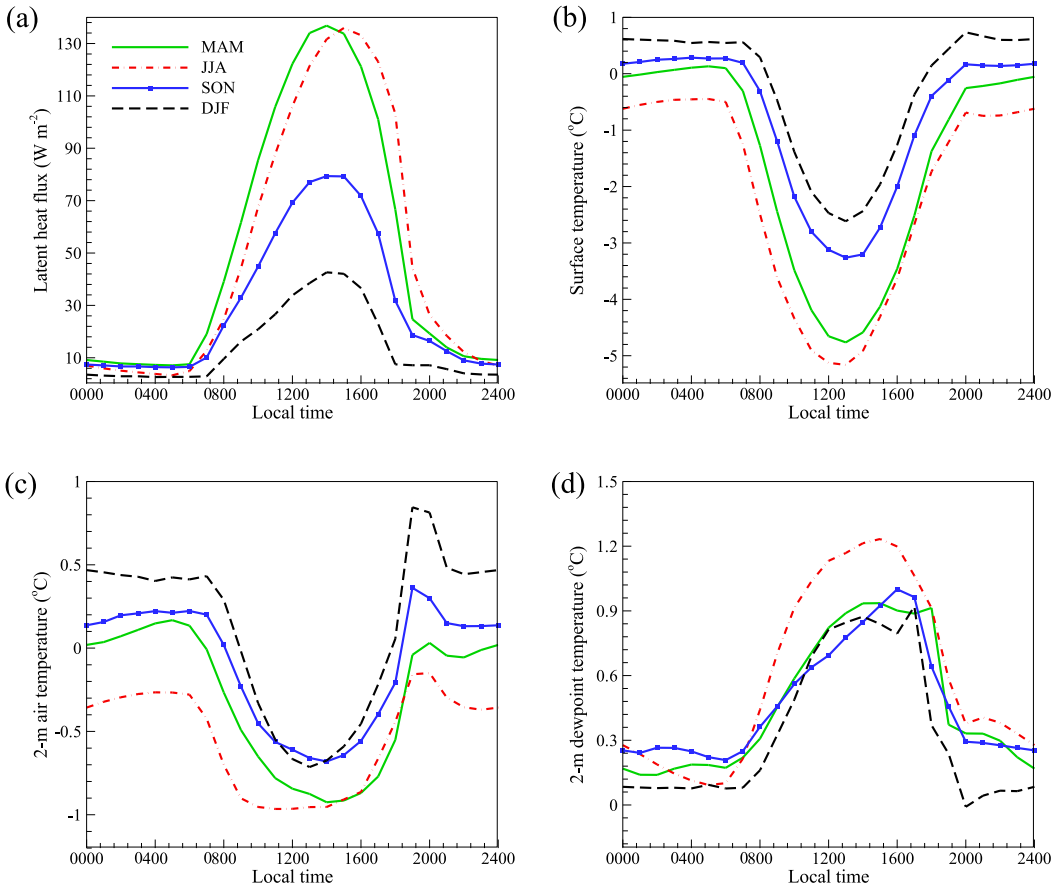

FIG. 14. Diurnal variation of average impact of green roofs on (a) LE, (b) T_s, (c) T_2, and (d) T_{d_2} over the entire Houston metropolitan area.

large-scale implementation. Finally, this study explores high-resolution numerical simulation of green roofs at the annual scale; we expect the findings to provide a useful guidance for sustainable development of other cities.

Acknowledgments. This work is supported by the National Science Foundation (NSF) under Grants CBET-1435881 and CBET-1444758 and the USDA-NIFA Agriculture and Food Research Initiative (Awards 2015-67003-23508 and 2015-67003-23460).

REFERENCES

Alexander, L., and Coauthors, 2006: Global observed changes in daily climate extremes of temperature and precipitation. *J. Geophys. Res.*, **111**, D05109, doi:10.1029/2005JD006290.

Arnfield, A. J., 2003: Two decades of urban climate research: A review of turbulence, exchanges of energy and water, and the urban heat island. *Int. J. Climatol.*, **23**, 1–26, doi:10.1002/joc.859.

Best, M. J., 2005: Representing urban areas within operational numerical weather prediction models. *Bound.-Layer Meteor.*, **114**, 91–109, doi:10.1007/s10546-004-4834-5.

Brubaker, K. L., and D. Entekhabi, 1996: Analysis of feedback mechanisms in land–atmosphere interaction. *Water Resour. Res.*, **32**, 1343–1357, doi:10.1029/96WR00005.

Carter, T., and C. R. Jackson, 2007: Vegetated roofs for stormwater management at multiple spatial scales. *Landscape Urban Plann.*, **80**, 84–94, doi:10.1016/j.landurbplan.2006.06.005.

Chen, F., and Coauthors, 2011: The integrated WRF/urban modelling system: Development, evaluation, and applications to urban environmental problems. *Int. J. Climatol.*, **31**, 273–288, doi:10.1002/joc.2158.

Cheng, W. Y., and W. J. Steenburgh, 2005: Evaluation of surface sensible weather forecasts by the WRF and the Eta models over the western United States. *Wea. Forecasting*, **20**, 812–821, doi:10.1175/WAF885.1.

Dodson, R., and D. Marks, 1997: Daily air temperature interpolated at high spatial resolution over a large mountainous region. *Climate Res.*, **8**, 1–20, doi:10.3354/cr008001.

Dudhia, J., 1989: Numerical study of convection observed during the winter monsoon experiment using a mesoscale two-dimensional model. *J. Atmos. Sci.*, **46**, 3077–3107, doi:10.1175/1520-0469(1989)046<3077:NSOCOD>2.0.CO;2.

Friedl, M. A., and Coauthors, 2002: Global land cover mapping from MODIS: Algorithms and early results. *Remote Sens. Environ.*, **83**, 287–302, doi:10.1016/S0034-4257(02)00078-0.

Fry, J. A., and Coauthors, 2011: Completion of the 2006 National Land Cover Database for the conterminous United States. *Photogramm. Eng. Remote Sensing*, **77**, 858–864.

Georgescu, M., 2015: Challenges associated with adaptation to future urban expansion. *J. Climate*, **28**, 2544–2563, doi:10.1175/JCLI-D-14-00290.1.

——, M. Moustaoui, A. Mahalov, and J. Dudhia, 2011: An alternative explanation of the semiarid urban area "oasis effect." *J. Geophys. Res.*, **116**, D24113, doi:10.1029/2011JD016720.

——, A. Mahalov, and M. Moustaoui, 2012: Seasonal hydroclimatic impacts of Sun Corridor expansion. *Environ. Res. Lett.*, **7**, 034026, doi:10.1088/1748-9326/7/3/034026.

——, P. E. Morefield, B. G. Bierwagen, and C. P. Weaver, 2014: Urban adaptation can roll back warming of emerging megapolitan regions. *Proc. Natl. Acad. Sci. USA*, **111**, 2909–2914, doi:10.1073/pnas.1322280111.

Grimmond, C. S. B., and Coauthors, 2010: The International Urban Energy Balance Models Comparison Project: First results from phase 1. *J. Appl. Meteor. Climatol.*, **49**, 1268–1292, doi:10.1175/2010JAMC2354.1.

——, and Coauthors, 2011: Initial results from phase 2 of the International Urban Energy Balance Model Comparison. *Int. J. Climatol.*, **31**, 244–272, doi:10.1002/joc.2227.

Hong, S.-Y., Y. Noh, and J. Dudhia, 2006: A new vertical diffusion package with an explicit treatment of entrainment processes. *Mon. Wea. Rev.*, **134**, 2318–2341, doi:10.1175/MWR3199.1.

IPCC, 2012: *Managing the Risks of Extreme Events and Disasters to Advance Climate Change Adaptation*. Cambridge University Press, 582 pp.

Kain, J. S., 2004: The Kain–Fritsch convective parameterization: An update. *J. Appl. Meteor.*, **43**, 170–181, doi:10.1175/1520-0450(2004)043<0170:TKCPAU>2.0.CO;2.

Krayenhoff, E. S., A. Christen, A. Martilli, and T. R. Oke, 2014: A multi-layer radiation model for urban neighbourhoods with trees. *Bound.-Layer Meteor.*, **151**, 139–178, doi:10.1007/s10546-013-9883-1.

Kripalani, R. H., J. H. Oh, A. Kulkarni, S. S. Sabade, and H. S. Chaudhari, 2007: South Asian summer monsoon precipitation variability: Coupled climate model simulations and projections under IPCC AR4. *Theor. Appl. Climatol.*, **90**, 133–159, doi:10.1007/s00704-006-0282-0.

Kusaka, H., H. Kondo, Y. Kikegawa, and F. Kimura, 2001: A simple single-layer urban canopy model for atmospheric models: Comparison with multi-layer and slab models. *Bound.-Layer Meteor.*, **101**, 329–358, doi:10.1023/A:1019207923078.

——, F. Chen, M. Tewari, J. Dudhia, D. O. Gill, M. G. Duda, W. Wang, and Y. Miya, 2012: Numerical simulation of urban heat island effect by the WRF Model with 4-km grid increment: An inter-comparison study between the urban canopy model and slab model. *J. Meteor. Soc. Japan*, **90B**, 33–45, doi:10.2151/jmsj.2012-B03.

Li, D., E. Bou-Zeid, and M. Oppenheimer, 2014: The effectiveness of cool and green roofs as urban heat island mitigation strategies. *Environ. Res. Lett.*, **9**, 055002, doi:10.1088/1748-9326/9/5/055002.

Lin, C.-Y., F. Chen, J. C. Huang, W. C. Chen, Y. A. Liou, W. N. Chen, and S.-C. Liu, 2008: Urban heat island effect and its impact on boundary layer development and land–sea circulation over northern Taiwan. *Atmos. Environ.*, **42**, 5635–5649, doi:10.1016/j.atmosenv.2008.03.015.

Martilli, A., A. Clappier, and M. Rotach, 2002: An urban surface exchange parameterisation for mesoscale models. *Bound.-Layer Meteor.*, **104**, 261–304, doi:10.1023/A:1016099921195.

Meehl, G. A., and C. Tebaldi, 2004: More intense, more frequent, and longer lasting heat waves in the 21st century. *Science*, **305**, 994–997, doi:10.1126/science.1098704.

Miao, S., and F. Chen, 2008: Formation of horizontal convective rolls in urban areas. *Atmos. Res.*, **89**, 298–304, doi:10.1016/j.atmosres.2008.02.013.

——, and ——, 2014: Enhanced modeling of latent heat flux from urban surfaces in the Noah/single-layer urban canopy coupled model. *Sci. China Earth Sci.*, **57**, 2408–2416, doi:10.1007/s11430-014-4829-0.

Mlawer, E. J., S. J. Taubman, P. D. Brown, M. J. Iacono, and S. A. Clough, 1997: Radiative transfer for inhomogeneous atmospheres: RRTM, a validated correlated-*k* model for the longwave. *J. Geophys. Res.*, **102**, 16 663–16 682, doi:10.1029/97JD00237.

Perkins, S., A. Pitman, N. Holbrook, and J. McAneney, 2007: Evaluation of the AR4 climate models' simulated daily maximum temperature, minimum temperature, and precipitation over Australia using probability density functions. *J. Climate*, **20**, 4356–4376, doi:10.1175/JCLI4253.1.

Poulos, G. S., and Coauthors, 2002: CASES-99: A comprehensive investigation of the stable nocturnal boundary layer. *Bull. Amer. Meteor. Soc.*, **83**, 555–581, doi:10.1175/1520-0477(2002)083<0555:CACIOT>2.3.CO;2.

Ramamurthy, P., E. Bou-Zeid, J. A. Smith, Z. Wang, M. L. Baeck, N. Z. Saliendra, J. L. Hom, and C. Welty, 2014: Influence of subfacet heterogeneity and material properties on the urban surface energy budget. *J. Appl. Meteor. Climatol.*, **53**, 2114–2129, doi:10.1175/JAMC-D-13-0286.1.

Rowe, D. B., 2011: Green roofs as a means of pollution abatement. *Environ. Pollut.*, **159**, 2100–2110, doi:10.1016/j.envpol.2010.10.029.

Sailor, D. J., 2008: A green roof model for building energy simulation programs. *Energy Build.*, **40**, 1466–1478, doi:10.1016/j.enbuild.2008.02.001.

Salamanca, F., A. Martilli, M. Tewari, and F. Chen, 2011: A study of the urban boundary layer using different urban parameterizations and high-resolution urban canopy parameters with WRF. *J. Appl. Meteor. Climatol.*, **50**, 1107–1128, doi:10.1175/2010JAMC2538.1.

Seto, K. C., M. Fragkias, B. Güneralp, and M. K. Reilly, 2011: A meta-analysis of global urban land expansion. *PLoS One*, **6**, e23777, doi:10.1371/journal.pone.0023777.

Skamarock, W. C., and J. B. Klemp, 2008: A time-split nonhydrostatic atmospheric model for weather research and forecasting applications. *J. Comput. Phys.*, **227**, 3465–3485, doi:10.1016/j.jcp.2007.01.037.

Song, J., and Z.-H. Wang, 2015a: Interfacing the urban land–atmosphere system through coupled urban canopy and atmospheric models. *Bound.-Layer Meteor.*, **154**, 427–448, doi:10.1007/s10546-014-9980-9.

——, and ——, 2015b: Impacts of mesic and xeric urban vegetation on outdoor thermal comfort and microclimate in Phoenix, AZ. *Build. Environ.*, **94**, 558–568, doi:10.1016/j.buildenv.2015.10.016.

Sun, T., E. Bou-Zeid, Z.-H. Wang, E. Zerba, and G.-H. Ni, 2013: Hydrometeorological determinants of green roof performance via a vertically-resolved model for heat and water transport. *Build. Environ.*, **60**, 211–224, doi:10.1016/j.buildenv.2012.10.018.

Sunwoo, Y., C. Chou, J. Takeshita, M. Murakami, and Y. Tochihara, 2006a: Physiological and subjective responses to low relative humidity. *J. Physiol. Anthropol.*, **25**, 7–14, doi:10.2114/jpa2.25.7.

——, ——, ——, ——, and ——, 2006b: Physiological and subjective responses to low relative humidity in young and elderly men. *J. Physiol. Anthropol.*, **25**, 229–238, doi:10.2114/jpa2.25.229.

Thompson, G., P. R. Field, R. M. Rasmussen, and W. D. Hall, 2008: Explicit forecasts of winter precipitation using an improved bulk microphysics scheme. Part II: Implementation of a new snow parameterization. *Mon. Wea. Rev.*, **136**, 5095–5115, doi:10.1175/2008MWR2387.1.

Unkašević, M., O. Jovanović, and T. Popović, 2001: Urban–suburban/rural vapour pressure and relative humidity differences at fixed hours over the area of Belgrade city. *Theor. Appl. Climatol.*, **68**, 67–73, doi:10.1007/s007040170054.

Vahmani, P., and T. S. Hogue, 2014: Incorporating an urban irrigation module into the Noah land surface model coupled with an urban canopy model. *J. Hydrometeor.*, **15**, 1440–1456, doi:10.1175/JHM-D-13-0121.1.

VanWoert, N. D., D. B. Rowe, J. A. Andresen, C. L. Rugh, R. T. Fernandez, and L. Xiao, 2005: Green roof stormwater retention. *J. Environ. Qual.*, **34**, 1036–1044, doi:10.2134/jeq2004.0364.

Wang, Z.-H., 2014a: A new perspective of urban–rural differences: The impact of soil water advection. *Urban Climate*, **10**, 19–34, doi:10.1016/j.uclim.2014.08.004.

——, 2014b: Monte Carlo simulations of radiative heat exchange in a street canyon with trees. *Sol. Energy*, **110**, 704–713, doi:10.1016/j.solener.2014.10.012.

——, E. Bou-Zeid, S. K. Au, and J. A. Smith, 2011a: Analyzing the sensitivity of WRF's single-layer urban canopy model to parameter uncertainty using advanced Monte Carlo simulation. *J. Appl. Meteor. Climatol.*, **50**, 1795–1814, doi:10.1175/2011JAMC2685.1.

——, ——, and J. A. Smith, 2011b: A spatially-analytical scheme for surface temperatures and conductive heat fluxes in urban canopy models. *Bound.-Layer Meteor.*, **138**, 171–193, doi:10.1007/s10546-010-9552-6.

——, ——, and ——, 2013: A coupled energy transport and hydrological model for urban canopies evaluated using a wireless sensor network. *Quart. J. Roy. Meteor. Soc.*, **139**, 1643–1657, doi:10.1002/qj.2032.

——, X. Zhao, J. Yang, and J. Song, 2016: Cooling and energy saving potentials of shade trees and urban lawns in a desert city. *Appl. Energy*, **161**, 437–444, doi:10.1016/j.apenergy.2015.10.047.

Yang, J., and Z.-H. Wang, 2014: Physical parameterization and sensitivity of urban hydrological models: Application to green roof systems. *Build. Environ.*, **75**, 250–263, doi:10.1016/j.buildenv.2014.02.006.

——, and ——, 2015: Optimizing urban irrigation schemes for the trade-off between energy and water consumption. *Energy Build.*, **107**, 335–344, doi:10.1016/j.enbuild.2015.08.045.

——, Q. Yu, and P. Gong, 2008: Quantifying air pollution removal by green roofs in Chicago. *Atmos. Environ.*, **42**, 7266–7273, doi:10.1016/j.atmosenv.2008.07.003.

——, Z.-H. Wang, F. Chen, S. Miao, M. Tewari, J. Voogt, and S. Myint, 2015a: Enhancing hydrologic modelling in the coupled Weather Research and Forecasting–urban modelling system. *Bound.-Layer Meteor.*, **155**, 87–109, doi:10.1007/s10546-014-9991-6.

——, ——, and K. E. Kaloush, 2015b: Environmental impacts of reflective materials: Is high albedo a 'silver bullet' for mitigating urban heat island? *Renew. Sustain. Energy Rev.*, **47**, 830–843, doi:10.1016/j.rser.2015.03.092.